GEOCHEMISTRY

Kimberlite genesis from a common carbonate-rich primary melt modified by lithospheric mantle assimilation

Andrea Giuliani[1,2,3]*, D. Graham Pearson[4], Ashton Soltys[1], Hayden Dalton[1], David Phillips[1], Stephen F. Foley[2], Emilie Lim[1], Karsten Goemann[5], William L. Griffin[2], Roger H. Mitchell[6]

Quantifying the compositional evolution of mantle-derived melts from source to surface is fundamental for constraining the nature of primary melts and deep Earth composition. Despite abundant evidence for interaction between carbonate-rich melts, including diamondiferous kimberlites, and mantle wall rocks en route to surface, the effects of this interaction on melt compositions are poorly constrained. Here, we demonstrate a robust linear correlation between the Mg/Si ratios of kimberlites and their entrained mantle components and between Mg/Fe ratios of mantle-derived olivine cores and magmatic olivine rims in kimberlites worldwide. Combined with numerical modeling, these findings indicate that kimberlite melts with highly variable composition were broadly similar before lithosphere assimilation. This implies that kimberlites worldwide originated by partial melting of compositionally similar convective mantle sources under comparable physical conditions. We conclude that mantle assimilation markedly alters the major element composition of carbonate-rich melts and is a major process in the evolution of mantle-derived magmas.

INTRODUCTION

Kimberlites are carbonate-rich volcanic rocks derived from low-degree melting of the mantle, which have a unique place in the Earth Sciences, because they represent the deepest sourced melts [>150 to 250 km; e.g., (1, 2)] and are the major host for diamonds. On their journey to the surface, kimberlite magmas entrain a range of mantle and crustal fragments, which provide unrivaled insights into the composition of the lithosphere and, occasionally, the convective upper mantle beneath continents through time. The hybrid nature of kimberlite rocks, combined with their ubiquitous alteration by fluids of diverse origin [both magmatic and crustal; e.g., (3)], makes the identification of primary kimberlite melt compositions challenging.

There is extensive petrographic and experimental evidence that kimberlite magmas interact with and assimilate entrained mantle material en route to the surface (4–11). It has been suggested that this assimilation process might be instrumental in driving the ascent of kimberlite magmas, whereby CO_2 exsolution in response to the assimilation of orthopyroxene enhances magma buoyancy (7). Although some experiments have confirmed an increase in melt SiO_2 due to orthopyroxene dissolution (9, 11), other experiments indicate that the solubility of silicate minerals in carbonate melts is low at high pressure (>3.5 GPa) and temperature [≥1200°C; (9, 12)]. Therefore, a fundamental, as yet unanswered, question is to what extent the assimilation of mantle material has influenced the com-

positional variability of kimberlite and other carbonate-rich melts that reach Earth's surface. If it is possible to "see through" the effects of lithospheric mantle assimilation and determine the compositions of primary kimberlite melts, these data should provide key insights into the compositional evolution of the convective mantle in space and time, as well as melting processes in the deep Earth. Furthermore, mantle assimilation might play a similarly major role in the petrogenesis of other mantle-derived magmas, especially those that at depth are enriched in CO_2 (e.g., melilitites, ultramafic lamprophyres, and some olivine lamproites), due to the high reactivity of carbonate-rich melts and mantle rocks (4, 6–9, 11–14).

To address the potential role of mantle assimilation in kimberlite petrogenesis, we have adopted two strategies. Initially, we compare the bulk compositions of kimberlites from representative localities with those of entrained peridotite xenoliths from the underlying lithospheric mantle (fig. S1 and table S1). We then compare the compositions of the xenocrystic cores and magmatic rims of kimberlitic olivine, the most abundant phase in fresh kimberlites (~50 volume %) from worldwide localities (fig. S1 and table S1). Analyses of olivine core compositions provide information on the nature of the mantle column traversed by kimberlite magmas. In contrast, olivine rim compositions represent proxies of the kimberlite melt composition after the assimilation of lithospheric material. These two approaches emphasize the controlling effects of the local lithospheric mantle on the nature of the erupted magmatic products.

RESULTS

Bulk kimberlite versus mantle peridotite compositions

The average Mg/Si ratios for bulk kimberlites from 10 on- and off-craton locations in southern Africa, Canada, West Greenland, and Siberia are compared with the average Mg/Si ratios of their entrained coarse-grained, well-equilibrated peridotite xenoliths from these same localities in Fig. 1. The Mg/Si ratio was chosen because it is indicative of the relative amount of olivine and orthopyroxene
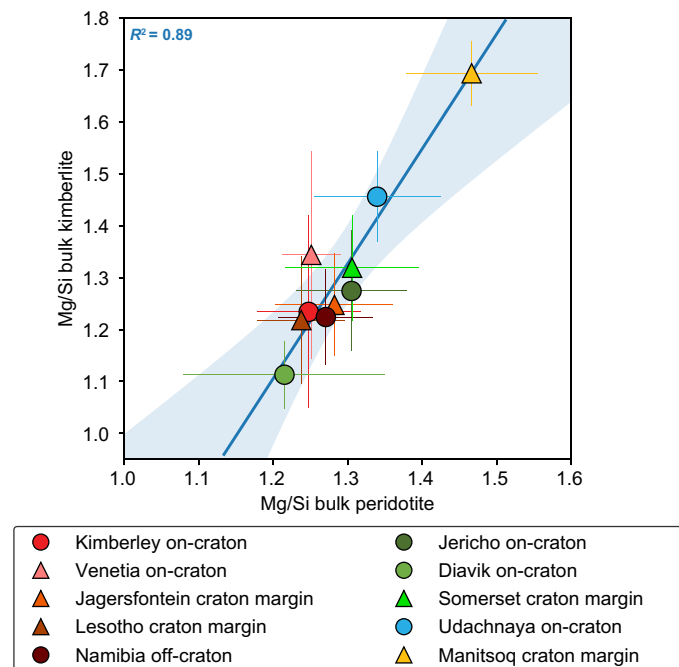
Fig. 1. Comparison between Mg/Si ratios of bulk kimberlite rocks and entrained mantle peridotites. Each data point is the average Mg/Si for multiple samples with the symbol bars indicating 2 SDs of the mean (see table S1). The blue line (with error envelope) is the linear regression through the data points and is calculated considering the uncertainties of both variables.
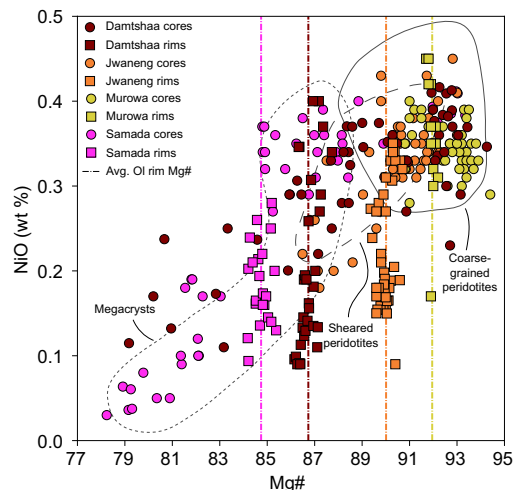

Fig. 2. Mg# versus NiO (wt %) concentrations in olivine cores and rims from the Damtshaa (Orapa, Botswana), Jwaneng (Botswana), Murowa (Zimbabwe), and Samada (Kaalvallei, South Africa) kimberlites. The fields of olivine (Ol) in coarse-grained and sheared peridotite xenoliths in kimberlites worldwide and olivine megacrysts from southern African kimberlites are shown for comparison (10). Dotted vertical bars are average rim compositions. Note that lower rim Mg# correspond to higher abundances of low-Mg# cores probably derived from megacrysts and sheared peridotites. Samada olivine data are from Lim *et al.* (25).

in the lithospheric mantle, which has been shown to vary widely in different regions [e.g., (15)]. In addition, kimberlite melt differentiation via olivine (± spinel) fractionation and accumulation of olivine in kimberlite rocks do not substantially alter bulk kimberlite Mg/Si (16). For example, the Mg/Si ratio (by weight) of the estimated primary melt parental to the Bultfontein kimberlite is 1.52 ± 0.10 [1 SD; (17)], whereas olivine (xenocrystic) cores and (magmatic) rims in this kimberlite have Mg/Si values of 1.56 ± 0.06 and 1.53 ± 0.02, respectively (10). Although crustal contamination of kimberlites is known to affect Si and Mg (16, 18), the analyses included in this compilation only refer to hypabyssal samples and have been screened for crustal contamination following the criteria outlined by Kjarsgaard *et al.* (18). Kimberlite bulk compositions were not corrected for contamination by mantle-derived xenocrystic material and, therefore, represent mixtures of magmatic components and mantle fragments. No filtering was applied to the peridotite bulk rock datasets.

The Mg/Si ratio in bulk kimberlite compositions is correlated with the Mg/Si of associated entrained peridotite xenoliths ($R^2 = 0.89$, $n = 10$; Fig. 1), as indicated by the results of Student's *t* test [$t_{calc} = 8.02 \gg t_{crit\ (0.01;\ 10)} = 3.17$; see Materials and Methods]. This linear correlation is a clear evidence of the control exerted by the local mantle lithosphere on the composition of kimberlite rocks in the crust [see also (16)], particularly with respect to the olivine/orthopyroxene ratio in the mantle, which is proportional to peridotite Mg/Si ratios (15). Mantle-derived olivine xenocrysts comprise a volumetrically major component of most kimberlites [~20 to 30 volume % or more; (17, 19–21)]. Therefore, bulk compositional data alone cannot differentiate between physical entrainment versus

assimilation of peridotitic material into the evolving kimberlite melt. Further insights can be gained by comparing the compositions of mantle-derived xenocrystic cores with the magmatic rims of olivine grains in kimberlites.

Olivine composition in kimberlites

We have analyzed major element compositions of olivine ($n \sim 1000$) in 22 kimberlites from South Africa, Botswana, Lesotho, Zimbabwe, Canada, Finland, and India, complemented by previously published data for 27 kimberlites from southern Africa, North America, Russia, India, Brazil, and Greenland (fig. S1 and table S1). This compilation is restricted to archetypal (formerly Group I) kimberlites from both on- and off-craton localities, with ages between ~1635 and 49 million years (Ma).

Olivine grains in kimberlites are typically zoned, regardless of morphology and size (fig. S2) [(10) and references therein]. Olivine cores have angular to more rounded shapes with occasional embayments and may host inclusions of mantle phases [e.g., clinopyroxene and garnet; (6, 21)] that are unstable in kimberlite magmas at low pressure. In each kimberlite, the olivine cores exhibit variable compositions. For example, the Mg# [= $100 \times Mg/(Mg + Fe)$] for olivine cores ranges from 79.2 to 94.3 ($n = 54$) for the Damtshaa (Orapa cluster, Botswana) kimberlite versus 90.8 to 94.4 ($n = 37$) for the Murowa kimberlite (Zimbabwe; Fig. 2). These compositions range from those typical of olivine in well-equilibrated, coarse-grained mantle peridotites (i.e., Mg# ~ 90 to 94) to more Fe-rich compositions (as low as Mg# = 78; Fig. 2). These features indicate derivation of olivine cores from the disaggregation of typical mantle peridotites, as well as other mantle lithologies that are more enriched in Fe, i.e., megacrysts and some sheared peridotites (10, 19–25), which derive from complex processes of hybridization between earlier kimberlite (or related) melts and peridotite wall rocks [e.g., (26–28)]. Some cores could also derive from the crystallization of failed

kimberlite intrusions at mantle depths (*29, 30*) or from disaggregation of "replacive" dunites where interaction with earlier kimberlite melts promoted olivine formation at the expense of other silicate phases (*31*). These products of earlier kimberlite melt rock reaction essentially become local lithospheric mantle wall rock.

Olivine rims often develop euhedral habits and contain inclusions of primary groundmass phases (e.g., spinel and ilmenite). Olivine rims exhibit a remarkably homogeneous Mg# composition at each locality (e.g., Damtshaa: 86.7 ± 0.4, *n* = 32; Murowa: 92.0 ± 0.1, *n* = 13), whereas Ni and Cr decrease, and Mn and Ca contents increase approaching grain margins (Fig. 2 and fig. S6) [(*10*) and references therein]. These characteristics are consistent with a magmatic origin for the olivine rims. The homogeneous Mg# value of olivine rims in each kimberlite implies that this parameter is insensitive to fractional crystallization, which is known to modify the composition of kimberlite and other magmas [e.g., (*16*)]. Furthermore, Lim *et al.* (*25*) recently showed that, in kimberlites from different continents, the Mg# of olivine rims is correlated with the abundance of magmatic phases (phlogopite and Fe-Ti oxides) in the kimberlite matrix, which largely crystallize upon magma emplacement in the upper crust. These lines of evidence suggest that olivine rim Mg# values can be used as proxies of kimberlite melt compositions after ascent through the lithospheric mantle.

The average Mg# of olivine rims are correlated with the mean (or median) Mg# of olivine cores from the same kimberlite [*n* = 49, R^2 = 0.73; t_{calc} = 11.27 ≫ $t_{critical(0.01, 49)}$ = 2.68; Fig. 3A and fig. S3]. This relationship implies that kimberlites with high-Mg olivine rims (e.g., Renard and Murowa) entrain xenocrystic cores and, therefore, mantle material that, on average, feature high Mg# (>92). For Murowa, this is consistent with the extreme depletion shown by peridotite xenoliths from this locality (*32*). Similarly, kimberlites

with Fe-rich olivine rims (e.g., Kaalvallei, Monastery, and Limpeza-18) have olivine cores with low Mg# (<90). As olivine compositions with Mg# < 90 are characteristic of megacrysts and sheared peridotites, the low-Mg# kimberlite melts preferentially sample mantle rocks that have previously interacted with earlier kimberlite or related melts. This relationship is supported by the inverse correlation [R^2 = 0.70, *n* = 49; t_{calc} = 10.47 ≫ $t_{critical(0.01, 49)}$ = 2.68] between the average Mg# of olivine rims and the fractional abundance of olivine cores with Mg# < 90 (Fig. 3B).

The correlation between olivine core and rim compositions is less strong, although still statistically significant, if mean NiO [R^2 = 0.30; t_{calc} = 4.49 > $t_{critical(0.01, 49)}$ = 2.68] or MnO [R^2 = 0.39; t_{calc} = 5.48 > $t_{critical(0.01, 49)}$ = 2.68] concentrations are used instead of Mg# (fig. S3). These more scattered correlations are unsurprising, given that mantle olivine typically contains relatively invariant Ni concentrations [between 0.3 and 0.4 weight % (wt %)], and Mn is only weakly correlated (inversely) with Mg# (*33*). Therefore, Mg# is the best indicator of the compositional variability of entrained (xenocrystic) olivine and, hence, of mantle material in kimberlites.

Kimberlites characterized by high-Mg olivine rims (i.e., Mg# > 90) cover the entire age range of this study [i.e., ~1635 Ma (Zero Satellite) to ~49 Ma (Aaron); fig. S4] and were emplaced well within inferred craton boundaries, with the exception of Jagersfontein, Buffelboudsfontein, and Zero Satellite, which are located along craton margins. In contrast, kimberlites with low-Mg olivine rims (i.e., Mg# < 87) are limited to Cretaceous occurrences located both on- and off-craton in southern Africa and Brazil. Whereas a highly depleted lithospheric mantle [typical of cratonic regions; e.g., (*15, 34*)] appears to be a prerequisite for the occurrence of kimberlites with high-Mg olivine, kimberlites with low-Mg olivine occurs throughout Archean and Proterozoic crust-mantle domains.
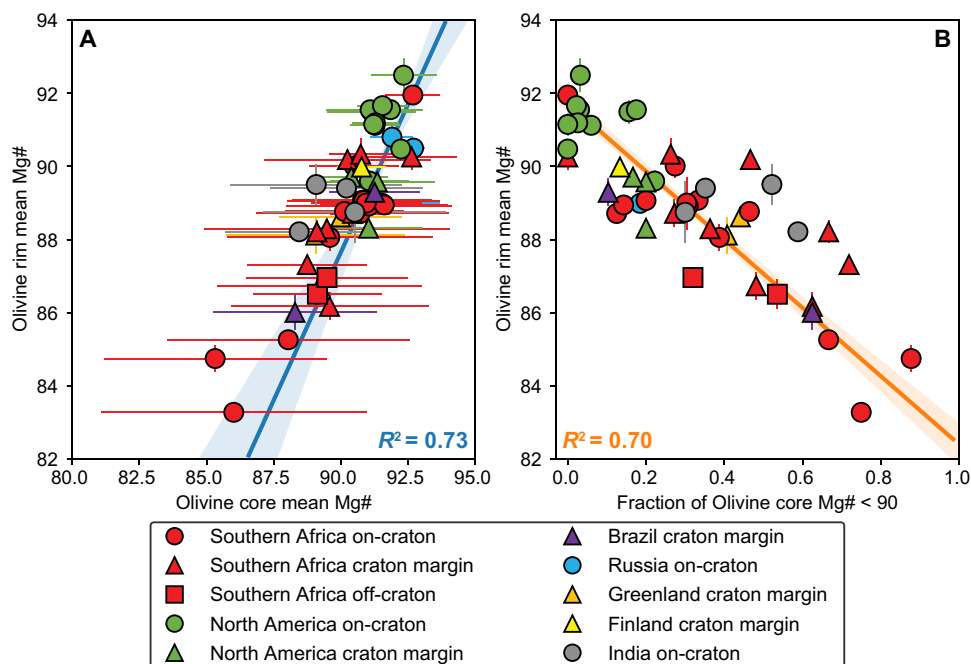

Fig. 3. Comparison of olivine core and rim major element compositions. (**A**) Average olivine rim Mg# versus average olivine core Mg# and (**B**) fraction of cores with Mg# < 90 in kimberlites from this and previous studies (see table S1). Symbol bars are 2 SDs of the mean. Blue and orange lines (with error envelopes) in (A) and (B), respectively, are the linear regressions through the data points and are calculated considering the uncertainties of *x* and *y* variables. For "Fraction of olivine core Mg# < 90," an arbitrary 2 SD of 0.1 is used for the regression calculations.

DISCUSSION

Lithospheric mantle assimilation controls the composition of kimberlites at surface

The linear correlations observed between the mean Mg# of olivine rims and cores (Fig. 3A) and the relative abundance of kimberlite-metasomatized cores (i.e., with Mg# < 90; Fig. 3B) in worldwide kimberlites point to a close relationship between the compositions of kimberlite melts and their entrained lithospheric mantle material. Possible reasons for this correlation include:

1) The olivine cores represent restite grains from the partially molten kimberlite source. This explanation is considered improbable given the large compositional range of the cores (e.g., Mg# = 79.2 to 94.3 at Damtshaa); in particular, low-Mg# compositions are unlikely to be of restite origin because partial melting residues feature elevated Mg#.

2) The olivine cores are early crystallization products of (failed) kimberlite intrusions at mantle depths (30, 31). Although this interpretation probably applies to some cores (e.g., low-Mg# compositions typical of olivine megacrysts) (24), the large compositional variation shown by olivine cores (e.g., Mg# = 78.2 to 93.4 at Samada) compared to the very narrow Mg# range for olivine rims in the same kimberlite (84.2 to 85.4 at Samada; Fig. 2) indicates that the bulk of the cores are unlikely to have crystallized from the same magmas that produced the olivine rim compositions.

3) The olivine cores, together with the other lithospheric mantle phases (orthopyroxene, clinopyroxene, and garnet), were entrained and partly assimilated from the wall rocks lining the kimberlite magmatic conduit. In this model, incorporation of lithospheric mantle material progressively alters the composition of transient kimberlite melts; consequently, magmatic olivine rims trend toward lower or higher Mg# depending on the average composition of mantle wall rocks. This interpretation is supported by the correlation between Mg/Si ratios of bulk kimberlite rocks and entrained mantle peridotites (Fig. 1), which implies that variable olivine/orthopyroxene (function of Mg/Si) ratios in the lithospheric mantle play an important role in kimberlite petrogenesis.

Kimberlite magmas that entrain and assimilate greater proportions of Fe-rich material (e.g., Samada, New Robinson and Monastery) become enriched in Fe, Mn, and Ti compared to their primary composition, which translates into lower Mg# olivine rims and higher modal abundances of Fe-Ti oxide phases and phlogopite in the matrix (25). The corollary is that the extent of interaction between earlier kimberlite (and related) melts and lithospheric mantle wall rock, which generates low-Mg# megacrysts, sheared peridotites, and other metasomatic lithologies (e.g., mantle polymict breccias) (29), dictates the level of enrichment in Fe, Mn, and Ti in the kimberlite melts that reach the surface. The absence of any correlation between olivine rim Mg# and Sr-Nd isotope compositions (fig. S5) shows that the assimilated material in low-Mg# kimberlites contains low concentrations of Sr and Nd compared to kimberlite melts and/or is not isotopically "enriched" (i.e., does not have high $^{87}Sr/^{86}Sr$ and low $^{143}Nd/^{144}Nd$, which are typical of phlogopite-rich mantle rocks) (35, 36). This lack of effect on the Sr-Nd isotope systems further testifies to the assimilation of incompatible element poor lithospheric mantle.

In summary, this work provides compelling geochemical evidence for assimilation of mantle material by carbonate-rich kimberlite melts. Previously, this process was only inferred from some experimental studies (7, 9, 11, 14) and from resorption textures in xenoliths and xenocrysts entrained by kimberlite magmas (4, 6, 8, 10). Our empirical observations, based on the compositions of xenocrystic and magmatic material from the same igneous rocks, unambiguously reveal that interaction with lithospheric material during ascent (together with other processes such as crystal fractionation and volatile loss) controls the major element composition of kimberlite melts emplaced into the crust. It seems plausible that this inference applies to any carbonate-rich melt that migrates through the mantle, due to the well-documented disequilibrium between carbonate-rich melts and lithospheric mantle peridotites at high pressure and temperature (7–9, 11, 13–14). Assimilation of lithospheric mantle material might be favored in highly reactive magmas, which ascend more slowly compared to kimberlites (e.g., lamproites and ultramafic lamprophyres) (37). Therefore, to constrain the primary composition(s) of mantle-derived magmas emplaced into the crust, which at depth are enriched in CO_2 (e.g., melilitites, ultramafic lamprophyres, some olivine lamproites and alkali basalts), it is necessary to quantify and remove the effects of interaction with the local lithospheric mantle using the available compositions of entrained xenocrysts. A quantitative approach toward this aim is provided below.

A common source for kimberlites

Deciphering the geochemical effects of mantle assimilation on the geochemistry of kimberlites is critical for constraining their source regions. Incompatible trace elements are less sensitive to the assimilation of mantle material than major and compatible trace elements, especially in kimberlite magmas, which contain very elevated levels of incompatible trace elements (16, 18). Fresh (or minimally altered) kimberlite rocks from worldwide localities show remarkably similar trace element patterns [Fig. 4; see also (38)]. Absolute concentrations fluctuate due to variable dilution of the magmatic component with xenocrystic material low in incompatible trace elements; however, the trace element patterns are analogous and include negative anomalies for K, Pb, Sr, Zr, Hf, and Ti in primitive mantle–normalized diagrams (Fig. 4). This observation implies that kimberlite magmas derive from broadly similar sources or that these magmas have equilibrated with a common mantle component. Kimberlites worldwide exhibit chondritic to moderately suprachondritic Nd and Hf isotope compositions, and pre-Mesozoic kimberlites have remarkably consistent close-to-chondritic Nd-Hf isotope compositions (39). These combined lines of evidence indicate kimberlite melt formation from similar sources located in the convective mantle. Possible contributions from subducted recycled material, as indicated by radiogenic isotope compositions (i.e., high $^{206}Pb/^{204}Pb$; negative ΔεHf) from Cretaceous-Eocene southern African, Brazilian, and western Canada (Lac de Gras) kimberlites (39, 40), appear to have had a limited impact on the trace element compositions of these kimberlite sources. The above interpretation is entirely consistent with the mantle-like oxygen isotope compositions of olivine in southern African, Brazilian, and Lac de Gras kimberlites (41) and the new constraints provided by olivine compositions. The linear correlation of Mg# between olivine cores and rims (Fig. 3A) can only be achieved if primary kimberlite melts have similar Mg# and, therefore, major element compositions before interacting with lithospheric mantle material.

On the basis of this constraint, it is possible to estimate the extent of lithospheric mantle assimilation by kimberlite melts, using mass balance calculations and the relative Mg# values of kimberlite
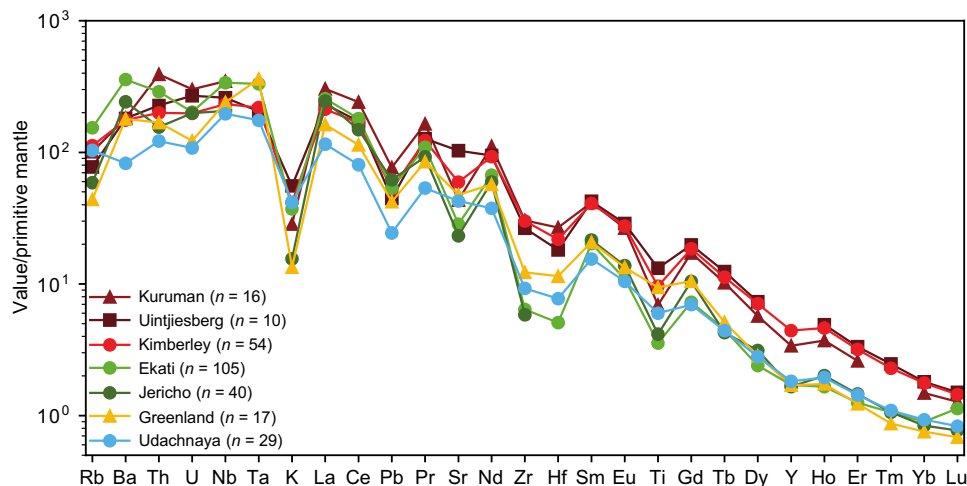
Fig. 4. Primitive mantle–normalized, incompatible trace element patterns of on- and off-craton kimberlites from different localities worldwide. Each data point is the average of multiple analyses as indicated in the key (see table S2). Note the similar shape of each pattern regardless of absolute trace element concentrations.

melt and assimilated material. In these calculations, the Mg# value of the estimated primary kimberlite melt (before interaction with the mantle lithosphere) is assumed to be 84 ± 1, which is the median value of previously estimated initial melt compositions (80 to 88) (16–18, 20, 42). The final kimberlite melts emplaced into the crust are assumed to be in equilibrium with the average compositions of olivine rims, reflecting the variability inherent to each locality. Melt Mg# values can be calculated using olivine rim Mg# and olivine melt D_{Fe-Mg} [0.50 ± 0.05; e.g., (43, 44)] for carbonate-rich melt compositions. These calculations show that, in the vast majority (44 of 49) of kimberlites studied, the Mg# of the final melt is lower than that of the primary melt (table S6). Using a lower olivine melt D_{Fe-Mg} of 0.4, yields decreased Mg# for all kimberlite melts due to interaction with the mantle lithosphere. This model implies that bulk assimilation of peridotitic material, which typically exhibits Mg# > 90 [e.g., (34)], cannot be the main cause of the compositional variability observed in kimberlite melts worldwide. Further insights can be gained by considering how kimberlite melts interact with peridotitic material.

Among the major rock-forming phases in mantle peridotites, orthopyroxene is the least stable in carbonate-rich melts. This inference is based on petrographic evidence of orthopyroxene resorption in kimberlites (6), the paucity of orthopyroxene compared to olivine xenocrysts in kimberlite rocks once the relative abundance of orthopyroxene versus olivine in mantle peridotites is considered (5), and results from experiments that have examined carbonate-rich melt compositions at variable pressure and temperature (7, 9, 11). These experiments show that, upon interaction with carbonate-rich melts at a pressure of <3.5 GPa, orthopyroxene melts incongruently to olivine + clinopyroxene + CO_2, with clinopyroxene later reacting with residual melt to generate further olivine and CO_2 (plus calcite) (9). These reactions involve a net loss of Mg from the carbonate-rich (kimberlite) melt (see Materials and Methods). Incongruent melting of orthopyroxene can therefore explain the decrease in Mg# (and MgO; table S7) inferred for most (if not all) of the kimberlite melts after interaction with lithospheric mantle wall rocks.

To quantify the amount of assimilated orthopyroxene in kimberlite melts from each locality, we undertook mass balance calculations with propagated uncertainties. The molar abundance of dissolved

orthopyroxene was calculated using the molar amount of Mg loss from the kimberlite melt after interaction with the lithospheric mantle, combined with the equations of Stone and Luth (9), which describe incongruent melting of orthopyroxene in carbonate-rich melts. Orthopyroxene compositions were computed from the average compositions of olivine cores and appropriate olivine-orthopyroxene distribution coefficients. Model details are provided in Materials and Methods. These simulations indicate that <15% and, more commonly, ≤10% (by mass) of orthopyroxene assimilation are required to produce the spectrum of kimberlite melt compositions emplaced in Earth's crust. Higher degrees of assimilation are obtained for kimberlites with low-Mg olivine (e.g., New Robinson and Monastery), which suggests preferential assimilation of less refractory Fe-rich material in kimberlite melts (where Fe-rich lithologies are available). Similar amounts (~7 to 8 wt %) of silicate mineral (orthopyroxene, clinopyroxene, and garnet) assimilation were estimated by Soltys et al. (17) for the Bultfontein kimberlite based on the modal abundance of olivine xenocrysts. However, we note that if bulk peridotite assimilation, which increases melt MgO contents, occurred in kimberlite melts before (e.g., deeper than) incongruent melting of orthopyroxene, then rates of orthopyroxene assimilation would be higher. Bulk peridotite assimilation may explain the elevated Mg# values calculated for some kimberlites with high-Mg olivine (e.g., Murowa and Renard; table S6).

From this modeling, it appears that assimilation of variable quantities of lithospheric mantle material by primary kimberlite melts of broadly similar composition can produce the wide range of kimberlite melt compositions (i.e., olivine rim Mg# = 83.3 to 92.3) observed at the surface. While assimilation of bulk peridotite appears to be important for those kimberlites that contain high-Mg olivine, incongruent melting of orthopyroxene could be the dominant mechanism that modify kimberlite melt compositions during interaction with the lithospheric mantle. Formation of peritectic olivine from orthopyroxene breakdown might also explain the occurrence of olivine cores with unusual compositions (i.e., elevated Mg# and CaO contents of >90 and >0.1 wt %, respectively) observed in kimberlites worldwide, which are uncharacteristic of any mantle lithology observed to date (10, 30). These assimilation processes increase silica contents (7, 9, 11) but have negligible effect on the

incompatible trace element compositions of kimberlite melts (e.g., see similar trace element patterns in Fig. 4) due to the low concentrations of these elements in orthopyroxene and bulk peridotite rocks. In addition, the lack of correlation between bulk kimberlite Mg/Si and mean Mg# of olivine rims (fig. S6), which is inversely correlated to the amount of assimilated orthopyroxene, suggests that bulk kimberlite compositions are largely controlled by physical entrainment of mantle material rather than assimilation of orthopyroxene and other mantle silicates.

In conclusion, bulk rock incompatible trace element and olivine compositions are both consistent with primary kimberlite melts being generated from similar convective mantle sources since at least ~1635 Ma. This interpretation agrees with the temporal uniformity of radiogenic isotope compositions in pre-Mesozoic kimberlites (39) and implies that the composition of kimberlite sources and their conditions of melting have not undergone major changes over time. Alternatively, all kimberlites have equilibrated with similar asthenospheric mantle before assimilation of lithospheric material. Similar incompatible trace element patters are also observed in some ocean island basalts (45, 46) and diamond fluid inclusions (47). Therefore, it seems likely that similar melts to those that generate kimberlites are involved in the formation of some diamonds and oceanic basalts, with the caveat that the final composition of kimberlites is influenced by extensive interaction with lithospheric mantle material. Our study demonstrates that the composition of kimberlite and, probably, other carbonate-rich melts that ascend through the mantle appears to be controlled by the local composition of the mantle that is entrained and partly assimilated. Future work should examine olivine lamproites and other magmatic rocks containing abundant xenocrystic and magmatic olivine to define the extent and mechanism(s) of lithospheric mantle assimilation in the petrogenesis of other low-volume, highly reactive melts from Earth's mantle.

MATERIALS AND METHODS

For this study of olivine compositions in kimberlites, we selected 24 samples from 22 kimberlites from southern Africa, Canada, Finland, and India (table S1). Sample selection was based on three criteria, namely, wide geographical and temporal coverage of kimberlite magmatism, absence of high-quality olivine compositional data in the literature, and occurrence of fresh olivine grains. With the exception of Peuyuk C (Somerset Island, Canada), which is a pyroclastic kimberlite, all the examined samples are hypabyssal. Olivine, locally partly serpentinized, is invariantly the most abundant phase (~40 to 60 volume %), and its size is highly variable from >1 mm to <100 μm. Only ≤1-mm-large grains tend to develop a euhedral habit.

Olivine grains for electron probe microanalysis (EPMA) were initially selected using a petrographic microscope rather than a scanning electron microscope [SEM; as recommended in (10)]. This approach was used to avoid bias toward evidently zoned grains and especially those with larger compositional (i.e., Mg#) and therefore visual contrast between cores and rims in back-scattered electron (BSE) images. Independent testing where several grains from the same thin section were selected by optical microscopy and using BSE images confirmed a bias toward core compositions with Mg# [= $100 \times Mg/(Mg + Fe)$] very different from the rims when BSE images were used. Selected grains cover the entire size range available in thin section, including large (>0.5 mm) anhedral/subhedral grains (also known as macrocrysts), and euhedral crystals of variable

size (i.e., >0.5-mm phenocrysts and <0.5-mm microphenocrysts). After selection, each grain was examined in BSE mode using a Philips (FEI) XL30 environmental SEM (University of Melbourne) to distinguish core, rim, and other compositionally distinct zones (internal zones between core and rim, external rinds). Some partly serpentinized grains did not have any rim preserved, and therefore, only their core was analyzed to obtain more representative average core compositions (rim Mg# is typically homogeneous in a given kimberlite). Some fresh grains did not display evident compositional zonation in BSE images, and for these grains, two analyses were performed corresponding to grain center and edge.

The major and minor element compositions of olivine were quantified by EPMA in two laboratories. At the University of Melbourne, we used a CAMECA SX-50 equipped with four wavelength dispersive spectrometers (WDS). Analytical conditions were as follows: beam acceleration voltage of 15 kV, beam current of 20 nA, beam diameter of 2 μm, and counting times per analysis of 20 s on peak positions and 10 s on two background positions located on either side of the peak position. Instrument calibration was undertaken using natural and synthetic materials, including wollastonite (Si-Kα and Ca-Kα), Cr metal (Cr-Kα), hematite (Fe-Kα), Mn metal (Mn-Kα), Mg oxide (Mg-Kα), and Ni metal (Ni-Kα). In addition, San Carlos olivine was included in the analytical sessions to evaluate the reproducibility of our olivine results (1 SD of San Carlos Mg# = 0.15, $n = 44$; table S4). Data reduction was performed using the PAP matrix correction software program. Typical quantification limits are ~0.02 wt % for NiO, MnO CaO, and Cr_2O_3. Analyses with lower concentrations (as low as 0.01 wt %) are however considered broadly representative of olivine compositions because they are consistent with data structure.

Additional analyses were undertaken at the Central Science Laboratory, University of Tasmania, using a JEOL JXA-8530F Plus field-emission electron microprobe equipped with five WDS and an energy dispersive spectrometer (EDS). Analytical conditions included an accelerating voltage of 15 kV, a beam current of 300 nA, and a beam diameter of 2 μm. The major elements Si, Fe, and Mg were simultaneously analyzed by EDS with one minor element (Al, Ca, Cr, Mn, and Ni) on each of the five WDS. Counting time was 90 s for all elements (on peak and background for WDS), corresponding to limit of quantification of 0.002 wt % for Al_2O_3, 0.003 wt % for Cr_2O_3, 0.005 wt % for NiO, 0.003 wt % for MnO, and 0.001 wt % for CaO. Instrument calibration was undertaken using natural minerals and synthetic oxides as reference standards (San Carlos olivine NMNH 111312-44 for Si-Kα, Fe-Kα, and Mg-Kα; natural corundum H 126097 for Al-Kα, natural wollastonite for Ca-Kα; synthetic Cr_2O_3 for Cr-Kα; natural rhodonite for Mn-Kα; and synthetic NiO for Ni-Kα,). Reproducibility of olivine Mg# values based on multiple analyses of San Carlos olivine is 0.07 (i.e., 1 SD of the mean, $n = 57$; table S4). The "Probe for EPMA" software (Probe Software Inc.) was used for acquisition and data reduction.

Analyses of cores, rims, BSE-unzoned grains and, where present, internal zones and rinds were plotted in conventional Mg# versus minor element (NiO, MnO, and CaO) compositional charts (fig. S6). Major element analyses revealed that all the analyzed grains that did not display zoning in BSE images were nonetheless zoned between core and rim of similar Mg# but distinct minor element compositions. No grains without xenocrystic core (i.e., "true phenocrysts") were encountered in this study, although they are known to occur in some kimberlites [(5, 10) and references therein]. Given the variable

origin of internal zones (i.e., mantle metasomatic products and liquidus olivine) (10, 23, 25), combined with their scarcity compared to ubiquitous rims, this study focused on the compositions of rims and cores. This approach has allowed us to obtain statistically significant datasets (i.e., >40 to 50 core and rim analyses) for most of the examined kimberlites and, at the same time, source abundant results from previous studies.
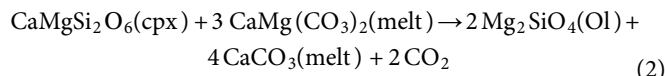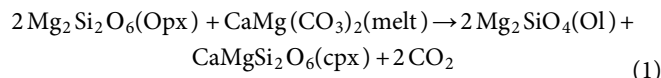
The new results were combined with the data reviewed and filtered for core and rim outliers by Giuliani (10). Additional results were recently published by Lim et al. (25) and Shaikh et al. (48), and these are also incorporated in this database for a total of 49 kimberlites from five continents with an age range between ~1635 and 49 Ma (table S1). Arithmetical means (and medians) and SDs of the means were calculated for cores and rims and are included in table S1.

The correlations observed between the compositions of olivine cores and rims (Fig. 3) were subjected to the standard two-tailed Student's t test for the null hypothesis, which the correlations between variable occurs by chance. We calculated t values at the 99% level of confidence using the relationship $t = r \times \sqrt{\frac{n-2}{1-r^2}}$, where n is the number of data points and r is the correlation coefficient. None of the correlations examined are likely to have occurred by chance because calculated t values are significantly higher than critical t values.
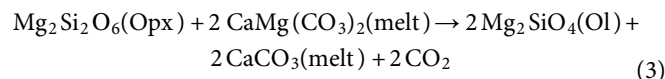
Mass balance calculations of orthopyroxene dissolution in kimberlite melts

To calculate the extent of orthopyroxene assimilation ("Ψ"), we have undertaken mass balance calculations using MgO variations in kimberlite melts due to interaction with lithospheric mantle wall rocks. Initial MgO concentrations (MgO$_{melt\,i}$ = 25 ± 2 wt %) in estimated primary kimberlite melts, i.e., before interaction with the lithosphere, are based on multiple estimates of initial kimberlite melt compositions (16–18, 20, 42). Final MgO abundances in the melt are calculated, assuming equilibrium with average olivine rim compositions, i.e., MgO$_{melt\,f}$ = MgO$_{olivine\,rim}$ × D$_{MgO}$, where D$_{MgO}$ is the MgO partition coefficient between olivine and melt. D$_{MgO}$ is calculated using high-pressure experiments of olivine in equilibrium with carbonate melts at $T = 1200°$ to $1400°C$ (43, 44). The combined results of these experiments returned a D$_{MgO}$ of 2.3 ± 0.4. Experiments of olivine in equilibrium with basaltic melts at these same temperatures show lower values (e.g., D$_{MgO}$ = 1.95 at 1200°C) (49). To account for the silicate-carbonate compositions of kimberlite melts [(17) and references therein], we have therefore adopted D$_{MgO}$ values of between 2.0 and 2.3. We note that the exact D$_{MgO}$ value is the largest source of uncertainty of this model because D$_{MgO}$ is dependent on crystallization temperature and melt composition, which are both loosely constrained for kimberlites.

These calculations show that MgO concentrations (and Mg# values; tables S6 and S7) of final kimberlite melts in equilibrium with olivine rims are typically lower than in primary kimberlite melts. This observation implies that bulk assimilation of peridotitic material, which typically has Mg# > 90 [e.g., (34)], cannot account for the compositional modification of kimberlite melts during interaction with the lithospheric mantle (with some potential exceptions). Orthopyroxene is widely known to be highly unstable in kimberlite melts (5–7) at a pressure of <3.5 GPa (9), and its breakdown in carbonate-rich (kimberlite) melts can be described using the equations of Stone and Luth (9)

$$2\,Mg_2Si_2O_6(Opx) + CaMg(CO_3)_2(melt) \rightarrow 2\,Mg_2SiO_4(Ol) + CaMgSi_2O_6(cpx) + 2\,CO_2 \tag{1}$$

$$CaMgSi_2O_6(cpx) + 3\,CaMg(CO_3)_2(melt) \rightarrow 2\,Mg_2SiO_4(Ol) + 4\,CaCO_3(melt) + 2\,CO_2 \tag{2}$$

Combining Eqs. 1 and 2, we obtain

$$Mg_2Si_2O_6(Opx) + 2\,CaMg(CO_3)_2(melt) \rightarrow 2\,Mg_2SiO_4(Ol) + 2\,CaCO_3(melt) + 2\,CO_2 \tag{3}$$

Equation 3 shows that for every mole of orthopyroxene dissolved in the carbonate-rich (kimberlite) melt, 2 moles of Mg are consumed in the melt to generate peritectic olivine. In principle, incongruent melting of orthopyroxene can therefore explain the decrease in MgO contents (and Mg#) computed for kimberlite melts after interaction with the lithospheric mantle.

The amount of orthopyroxene (Ψ) incongruently dissolved in kimberlite melts can be determined using Mg loss in kimberlite melts and the molar weight of orthopyroxene. The latter is computed using the ideal formula of orthopyroxene (Mg,Fe)$_2$Si$_2$O$_6$ with Mg/Fe$_{Opx}$ defined by the average Mg/Fe of (xenocrystic) olivine cores and the Mg# difference between orthopyroxene and olivine ("Opx-Ol Mg#"). Opx-Ol Mg# (0.9 ± 1.0) is derived from multiple analyses of olivine and orthopyroxene in several (n = 73) equilibrated mantle peridotites from the Kimberley (South Africa), Diavik (Canada), and Udachnaya-East (Russia) kimberlites (table S5) and is consistent with results from equilibrium experiments at high pressure and temperature [e.g., (50)]. Using pure enstatite rather than the calculated orthopyroxene compositions has a negligible role on Ψ values.

Values of Ψ and associated uncertainties were quantified using Monte Carlo simulations with fully propagated uncertainties, where each parameter was randomized and blocks of 1000 simulations were constructed for each parameter. The results of these computations are indistinguishable from those obtained using arithmetic formulas (i.e., without randomization), including those for error propagations, and we therefore only present the latter in table S7. Using olivine-melt D$_{MgO}$ of 2.3, the estimated amount of assimilated orthopyroxene varies between 8.1 (± 7.0) wt % and 14.6 (± 6.8) wt % (table S7) for end-member cases, i.e., high-Mg olivine (Murowa and Renard) and low-Mg olivine (New Robinson and Monastery), respectively (table S1). The extent of orthopyroxene assimilation increases with decreasing Mg# of olivine cores and rims (e.g., $\Psi = 13.4 ± 6.8$ for Monastery; $\Psi = 10.3 ± 7.0$ for Bultfontein; $\Psi = 8.1 ± 7.0$ for Murowa, and assuming that D$_{MgO}$ = 2.3) and by decreasing olivine melt D$_{MgO}$ to 2.0 ($\Psi_{max} = 7.1 ± 7.8$ and $\Psi_{min} = 0.0 ± 8.2$). These results suggest that up to 15% and, more commonly, ≤10% (by mass) of orthopyroxene can be dissolved in kimberlites to generate the spectrum of kimberlite melt compositions that reach the upper crust, assuming similar primary kimberlite melts. However, higher amounts of orthopyroxene can be dissolved if kimberlites assimilate bulk peridotite material in the deeper lithosphere.

SUPPLEMENTARY MATERIALS

REFERENCES AND NOTES

1. S. E. Haggerty, Superkimberlites: A geodynamic diamond window to the Earth's core. *Earth Planet. Sci. Lett.* **122**, 57–69 (1994).

2. D. G. Pearson, F. E. Brenker, F. Nestola, J. McNeill, L. Nasdala, M. T. Hutchison, S. Matveev, K. Mather, G. Silversmit, S. Schmitz, B. Vekemans, L. Vincze, Hydrous mantle transition zone indicated by ringwoodite included within diamond. *Nature* **507**, 221–224 (2014).

3. A. Giuliani, D. Phillips, V. S. Kamenesty, M. L. Fiorentini, J. Farquhar, M. A. Kendrick, Stable isotope (C, O, S) compositions of volatile-rich minerals in kimberlites: A review. *Chem. Geol.* **374–375**, 61–83 (2014).

4. R. H. Hunter, L. A. Taylor, Instability of garnet from the mantle: Glass as evidence of metasomatic melting. *Geology* **10**, 617–620 (1982).

5. R. H. Mitchell, Petrology of hypabyssal kimberlites: Relevance to primary magma compositions. *J. Volcanol. Geotherm. Res.* **174**, 1–8 (2008).

6. V. S. Kamenetsky, M. B. Kamenetsky, A. V. Sobolev, A. V. Golovin, V. V. Sharygin, N. P. Pokhilenko, N. V. Sobolev, Can pyroxenes be liquidus minerals in the kimberlite magma? *Lithos* **112**, 213–222 (2009).

7. J. K. Russell, L. A. Porritt, Y. Lavallee, D. B. Dingwell, Kimberlite ascent by assimilation-fuelled buoyancy. *Nature* **481**, 352–356 (2012).

8. A. Soltys, A. Giuliani, D. Phillips, V. S. Kamenetsky, R. Maas, J. Woodhead, T. Rodemann, In-situ assimilation of mantle minerals by kimberlitic magmas — Direct evidence from a garnet wehrlite xenolith entrained in the Bultfontein kimberlite (Kimberley, South Africa). *Lithos* **256–257**, 182–196 (2016).

9. R. S. Stone, R. W. Luth, Orthopyroxene survival in deep carbonatite melts: Implications for kimberlites. *Contrib. Mineral. Petrol.* **171**, 63 (2016).

10. A. Giuliani, Insights into kimberlite petrogenesis and mantle metasomatism from a review of the compositional zoning of olivine in kimberlites worldwide. *Lithos* **312-313**, 322–342 (2018).

11. I. S. Sharygin, K. D. Litasov, A. Shatskiy, O. G. Safonov, A. V. Golovin, E. Ohtani, N. P. Pokhilenko, Experimental constraints on orthopyroxene dissolution in alkali-carbonate melts in the lithospheric mantle: Implications for kimberlite melt composition and magma ascent. *Chem. Geol.* **455**, 44–56 (2017).

12. A. G. Sokol, A. N. Kruk, D. A. Chebotarev, Y. N. Palyanov, Carbonatite melt–peridotite interaction at 5.5–7.0 GPa: Implications for metasomatism in lithospheric mantle. *Lithos* **248–251**, 66–79 (2016).

13. D. H. Green, M. E. Wallace, Mantle metasomatism by ephemeral carbonatite melts. *Nature* **336**, 459–462 (1988).

14. V. S. Kamenetsky, G. M. Yaxley, Carbonate–silicate liquid immiscibility in the mantle propels kimberlite magma ascent. *Geochim. Cosmochim. Acta* **158**, 48–56 (2015).

15. D. G. Pearson, N. Wittig, The mantle and core, in *Treatise on Geochemistry (Second Edition)*, H. D. Holland, K. K. Turekian, Eds. (Elsevier, Oxford, 2014), vol. 3, pp. 255–292.

16. A. P. le Roex, D. R. Bell, P. Davis, Petrogenesis of group I Kimberlites from Kimberley, South Africa: Evidence from bulk-rock geochemistry. *J. Petrol.* **44**, 2261–2286 (2003).

17. A. Soltys, A. Giuliani, D. Phillips, A new approach to reconstructing the composition and evolution of kimberlite melts: A case study of the archetypal Bultfontein kimberlite (Kimberley, South Africa). *Lithos* **304–307**, 1–15 (2018).

18. B. A. Kjarsgaard, D. G. Pearson, S. Tappe, G. M. Nowell, D. P. Dowall, Geochemistry of hypabyssal kimberlites from Lac de Gras, Canada: Comparisons to a global database and applications to the parent magma problem. *Lithos* **112**, 236–248 (2009).

19. R. C. Brett, J. K. Russell, S. Moss, Origin of olivine in kimberlite: Phenocryst or impostor? *Lithos* **112**, 201–212 (2009).

20. T. F. D. Nielsen, K. K. Sand, The Majuagaa kimberlite dike, Maniitsoq region, West Greenland: Constraints on an Mg-rich silicocarbonatitic melt composition from groundmass mineralogy and bulk compositions. *Can. Mineral.* **46**, 1043–1061 (2008).

21. Y. Bussweiler, S. F. Foley, D. Prelević, D. E. Jacob, The olivine macrocryst problem: New insights from minor and trace element compositions of olivine from Lac de Gras kimberlites, Canada. *Lithos* **220–223**, 238–252 (2015).

22. V. S. Kamenetsky, M. B. Kamenetsky, A. V. Sobolev, A. V. Golovin, S. Demouchy, K. Faure, V. V. Sharygin, D. V. Kuzmin, Olivine in the Udachnaya-East Kimberlite (Yakutia, Russia): Types, compositions and origins. *J. Petrol.* **49**, 823–839 (2008).

23. G. H. Howarth, L. A. Taylor, Multi-stage kimberlite evolution tracked in zoned olivine from the Benfontein sill, South Africa. *Lithos* **262**, 384–397 (2016).

24. A. Moore, G. Costin, Kimberlitic olivines derived from the Cr-poor and Cr-rich megacryst suites. *Lithos* **258–259**, 215–227 (2016).

25. E. Lim, A. Giuliani, D. Phillips, K. Goemann, Origin of complex zoning in olivine from diverse, diamondiferous kimberlites and tectonic settings: Ekati (Canada), Alto Paranaiba (Brazil) and Kaalvallei (South Africa). *Mineral. Petrol.* **112**, 539–554 (2018).

26. J.-C. C. Mercier, *The Mantle Sample: Inclusion in Kimberlites and Other Volcanics* (American Geophysical Union, 1979), vol. 1, pp. 197–212.

27. Y. Bussweiler, D. G. Pearson, T. Stachel, B. A. Kjarsgaard, Cr-rich megacrysts of clinopyroxene and garnet from Lac de Gras kimberlites, Slave Craton, Canada –

28. D. A. Ionov, L. S. Doucet, P. A. E. Pogge von Strandmann, A. V. Golovin, A. V. Korsakov, Links between deformation, chemical enrichments and Li-isotope compositions in the lithospheric mantle of the central Siberian craton. *Chem. Geol.* **475**, 105–121 (2017).

29. A. Giuliani, D. Phillips, V. S. Kamenetsky, M. A. Kendrick, B. A. Wyatt, K. Goemann, G. Hutchinson, Petrogenesis of mantle polymict breccias: Insights into mantle processes coeval with kimberlite magmatism. *J. Petrol.* **55**, 831–858 (2014).

30. N. V. Sobolev, A. V. Sobolev, A. A. Tomilenko, S. V. Kovyazin, V. G. Batanova, D. V. Kuz'min, Paragenesis and complex zoning of olivine macrocrysts from unaltered kimberlite of the Udachnaya-East pipe, Yakutia: Relationship with the kimberlite formation conditions and evolution. *Russian Geol. Geophys.* **56**, 260–279 (2015).

31. N. T. Arndt, M. Guitreau, A.-M. Boullier, A. Le Roex, A. Tommasi, P. Cordier, A. Sobolev, Olivine, and the origin of kimberlite. *J. Petrol.* **51**, 573–602 (2010).

32. D. G. Pearson, C. B. Smith, J. Liu, K. A. Mather, M. Y. Krebs, G. P. Bulanova, A. Kobussen, Characteristics and origin of the mantle root beneath the Murowa diamond mine: Implications for craton and diamond formation. in *Geoscience and Exploration of the Argyle, Bunder, Diavik and Murowa Diamond Deposits* (Society of Economic Geologists, 2018), pp. 403–424.

33. J. C. M. De Hoog, L. Gall, D. H. Cornell, Trace-element geochemistry of mantle olivine and application to mantle petrogenesis and geothermobarometry. *Chem. Geol.* **270**, 196–215 (2010).

34. W. L. Griffin, S. Y. O'Reilly, J. C. Afonso, G. C. Begg, The composition and evolution of lithospheric mantle: A re-evaluation and its tectonic implications. *J. Petrol.* **50**, 1185–1204 (2009).

35. C. J. Hawkesworth, A. J. Erlank, P. D. Kempton, F. G. Waters, Mantle metasomatism: Isotope and trace-element trends in xenoliths from Kimberley, South Africa. *Chem. Geol.* **85**, 19–34 (1990).

36. A. Fitzpayne, A. Giuliani, R. Maas, J. Hergt, P. Janney, D. Phillips, Progressive metasomatism of the mantle by kimberlite melts: Sr–Nd–Hf–Pb isotope compositions of MARID and PIC minerals. *Earth Planet. Sci. Lett.* **509**, 15–26 (2019).

37. A. H. Peslier, A. B. Woodland, J. A. Wolff, Fast kimberlite ascent rates estimated from hydrogen diffusion profiles in xenolithic mantle olivines from southern Africa. *Geochim. Cosmochim. Acta* **72**, 2711–2722 (2008).

38. Y. Khazan, Y. Fialko, Why do kimberlites from different provinces have similar trace element patterns? *Geochem. Geophys. Geosyst.* **6**, Q10002 (2005).

39. J. D. Woodhead, J. Hergt, A. Giuliani, R. Maas, D. Phillips, D. G. Pearson, G. Nowell, Kimberlites reveal 2.5-billion-year evolution of a deep, isolated mantle reservoir. *Nature* **573**, 578–581 (2019).

40. C. B. Smith, Pb, Sr and Nd isotopic evidence for sources of southern African Cretaceous kimberlites. *Nature* **304**, 51–54 (1983).

41. A. Giuliani, L. A. J. Martin, A. Soltys, W. L. Griffin, Mantle-like oxygen isotopes in kimberlites determined by in situ SIMS analyses of zoned olivine. *Geochim. Cosmochim. Acta* **266**, 274–291 (2019).

42. S. E. Price, J. K. Russell, M. G. Kopylova, Primitive magma from the Jericho Pipe, N.W.T., Canada: Constraints on primary kimberlite melt chemistry. *J. Petrol.* **41**, 789–808 (2000).

43. J. A. Dalton, B. J. Wood, The compositions of primary carbonate melts and their evolution through wallrock reaction in the mantle. *Earth Planet. Sci. Lett.* **119**, 511–525 (1993).

44. G. P. Brey, V. K. Bulatov, A. V. Girnis, Influence of water and fluorine on melting of carbonated peridotite at 6 and 10 GPa. *Lithos* **112**, 249–259 (2009).

45. Y. Weiss, C. Class, S. L. Goldstein, T. Hanyu, Key new pieces of the HIMU puzzle from olivines and diamond inclusions. *Nature* **537**, 666–670 (2016).

46. S. E. Mazza, E. Gazel, M. Bizimis, R. Moucha, P. Béguelin, E. A. Johnson, R. J. McAleer, A. V. Sobolev, Sampling the volatile-rich transition zone beneath Bermuda. *Nature* **569**, 398–403 (2019).

47. Y. Weiss, W. L. Griffin, D. R. Bell, O. Navon, High-Mg carbonatitic melts in diamonds, kimberlites and the sub-continental lithosphere. *Earth Planet. Sci. Lett.* **309**, 337–347 (2011).

48. A. M. Shaikh, S. P. Kumar, S. C. Patel, S. S. Thakur, S. Ravi, D. Behera, The P3 kimberlite and P4 lamproite, Wajrakarur kimberlite field, India: Mineralogy, and major and minor element compositions of olivines as records of their phenocrystic vs xenocrystic origin. *Mineral. Petrol.* **112**, 609–624 (2018).

49. P. L. Roeder, R. F. Emslie, Olivine-liquid equilibrium. *Contrib. Mineral. Petrol.* **29**, 275–289 (1970).

50. V. von Seckendorff, H. S. C. O'Neill, An experimental study of Fe-Mg partitioning between olivine and orthopyroxene at 1173, 1273 and 1423 K and 1.6 GPa. *Contrib. Mineral. Petrol.* **113**, 196–207 (1993).

Citation: A. Giuliani, D. G. Pearson, A. Soltys, H. Dalton, D. Phillips, S. F. Foley, E. Lim, K. Goemann, W. L. Griffin, R. H. Mitchell, Kimberlite genesis from a common carbonate-rich primary melt modified by lithospheric mantle assimilation. *Sci. Adv.* **6**, eaaz0424 (2020).

ScienceAdvances

Kimberlite genesis from a common carbonate-rich primary melt modified by lithospheric mantle assimilation

Andrea Giuliani, D. Graham Pearson, Ashton Soltys, Hayden Dalton, David Phillips, Stephen F. Foley, Emilie Lim, Karsten Goemann, William L. Griffin and Roger H. Mitchell

ARTICLE TOOLS	http://advances.sciencemag.org/content/6/17/eaaz0424
SUPPLEMENTARY MATERIALS	http://advances.sciencemag.org/content/suppl/2020/04/20/6.17.eaaz0424.DC1
REFERENCES	This article cites 47 articles, 2 of which you can access for free http://advances.sciencemag.org/content/6/17/eaaz0424#BIBL
PERMISSIONS	http://www.sciencemag.org/help/reprints-and-permissions

Use of this article is subject to the Terms of Service